Broad Bandwidth, Self-Powered Acoustic Sensor Created by Dynamic Near-Field Electrospinning of Suspended, Transparent Piezoelectric Nanofiber Mesh

Author(s):
Wang, Wenyu; Stipp, Patrick N.; Ouaras, Karim; Fathi, Saeed; Huang, Yan Y.S.

Publication date:
2020-07-16

Permanent link:
https://doi.org/10.3929/ethz-b-000420939

Originally published in:
Small 16(28), https://doi.org/10.1002/smll.202000581

NANO · MICRO small
www.small-journal.com

Broad Bandwidth, Self-Powered Acoustic Sensor Created by Dynamic Near-Field Electrospinning of Suspended, Transparent Piezoelectric Nanofiber Mesh

*Wenyu Wang, Patrick N. Stipp, Karim Ouaras, Saeed Fathi, and Yan Yan Shery Huang**

Freely suspended nanofibers, such as spider silk, harnessing their small diameter (sub-micrometer) and spanning fiber morphology, behave as a nonresonating acoustic sensor. The associated sensing characteristics, departing from conventional resonant acoustic sensors, could be of tremendous interest for the development of high sensitivity, broadband audible sensors for applications in environmental monitoring, biomedical diagnostics, and internet-of-things. Herein, a low packing density, freely suspended nanofiber mesh with a piezoelectric active polymer is fabricated, demonstrating a self-powered acoustic sensing platform with broad sensitivity bandwidth covering 200–5000 Hz at hearing-safe sound pressure levels. Dynamic near-field electrospinning is developed to fabricate in situ poled poly(vinylidene fluoride-*co*-trifluoroethylene) (P(VDF-TrFE)) nanofiber mesh (average fiber diameter ≈307 nm), exhibiting visible light transparency greater than 97%. With the ability to span the nanomesh across a suspension distance of 3 mm with minimized fiber stacking (≈18% fiber packing density), individual nanofibers can freely imitate the acoustic-driven fluctuation of airflow in a collective manner, where piezoelectricity is harvested at two-terminal electrodes for direct signal collection. Applications of the nanofiber mesh in music recording with good signal fidelity are demonstrated.

Acoustic waves carry rich information in a wide frequency bandwidth from a few hertz to megahertz. The detection of acoustic signals holds important applications in a number of fields, ranging from environmental detection[1,2] to biomedical diagnostics.[3] The ability to efficiently detect acoustic signals through a broad audible frequency bandwidth could facilitate the development of emerging human–machine interaction devices,[4–6] such as electronic skin,[7,8] unmanned vehicle,[9] and cochlear implant.[10–12] Significant efforts have been invested in developing novel structures and new materials for next-generation acoustic sensors.[13–18] Despite these achievements, most existing acoustic sensors are resonant systems, and the sensing elements are designed to operate at a frequency bandwidth close to the resonant frequency of the devices. Thus, the associated sensitivity bandwidth is relatively narrow and constrained by the acoustic sensing elements (e.g., material and geometry). In addition, most of the presented micro-electromechanical system (MEMS) resonators work at the frequency range of a few kilohertz to megahertz.[19,20]

Instead of resonant acoustic sensing, freely suspended, long nanofibers could act as nonresonating acoustic sensors. For example, some sub-micron scale spider silks (e.g., *Araneus diadematus* spider silk) were shown to possess high sensitivity and efficiency in detecting sound waves from infrasound to ultrasound (1–50 kHz).[21] To recapitulate nonresonating systems such as the *A. diadematus* spider silk, the sensing elements need to be in the nanoscale, flexible, of low packing density, and free-standing so that their motions can be easily driven by the acoustic waves in the airflow at various frequencies.[22] Existing studies have employed far-field electrospinning (FFES) to produce suspended nanofibers made of poly(methyl methacrylate), but complex circuitry and an external power supply were needed to convert the acoustic information detected by this passive material.[23] Despite that the use of piezoelectric polymers could impart self-powered devices, seeing potentials for convenient field applications,[15,24,25] the piezoelectric nanofibers in most of the reported devices are in a highly stacked configuration with high packing density (almost 100%), resembling a solid porous film structure (film thickness of tens of micrometers).[16,26,27] Thus, the entire fiber mat is vibrating as an integrated, constrained system, so that individual nanofibers are not freely vibrating. In these cases, the characteristic length-scale determining the acoustic sensing performance is dominated by the thickness of the

W. Wang, P. N. Stipp, Dr. K. Ouaras, Dr. S. Fathi, Dr. Y. Y. S. Huang
The Nanoscience Center
Department of Engineering
University of Cambridge
Cambridge CB3 0FF, UK
E-mail: yysh2@cam.ac.uk
P. N. Stipp
Institute of Robotics and Intelligent Systems
Swiss Federal Institute of Technology Zurich (ETH)
Rämistrasse 101, Zürich 8092, Switzerland
The ORCID identification number(s) for the author(s) of this article can be found under https://doi.org/10.1002/smll.202000581.

DOI: 10.1002/smll.202000581

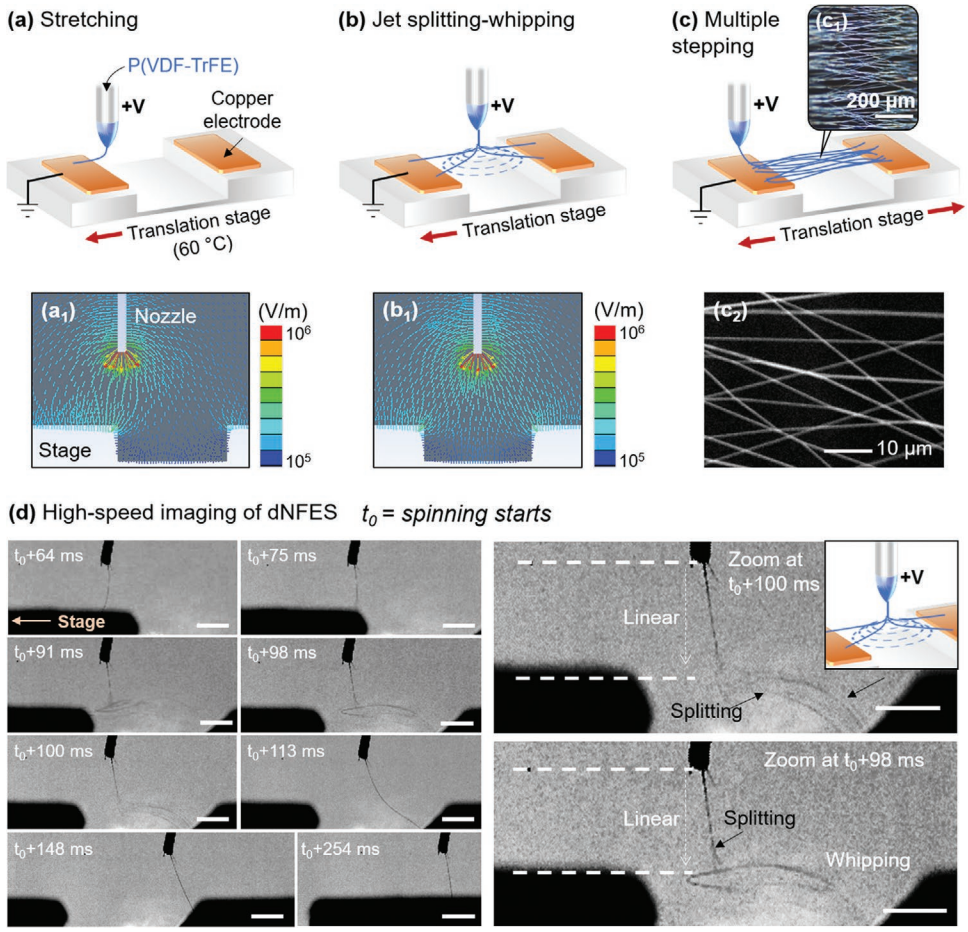

Figure 1. The process of dNFES. a) The dNFES setup consists of a heated translation stage with a pair of elevated electrodes. The high voltage between the needle and the electrodes initiates fiber spinning and stretches the fiber jet. a_1) Simulation showing the static electric field distribution. b) When the needle moves between the two elevated electrodes, fiber jet whips and splits due to competing static electric forces on both electrodes, as simulated in (b_1). c) Multiple stepping on both elevated electrodes creates a mesh of suspended nanofibers. c_1) Optical image and c_2) SEM image showing the suspended, directional fiber mesh at different magnifications. d) A series of high-speed images showing one cycle of the dNFES process, and zoomed-in pictures showing the jet splitting and whipping (scale bar: 1 mm).

entire fiber mat. In other words, internal resonance associated with the film structure would dominate the sensitive frequency bandwidth, and hence resulting in a narrow frequency bandwidth.

Herein, by using dynamic near-field electrospinning (dNFES), we fabricate a broad bandwidth acoustic sensor based on piezoelectric nanofiber mesh. The free-standing, low packing density (≈18%), air-permissive and oriented nanofibers span across a pair of parallel electrodes, acting as a nonresonating acoustic sensor. These high aspect ratio, lightweight, and flexible nanofibers do not have evident internal resonant frequencies. Instead, their motion could be easily driven by the airflow under the acoustic field. Upon the acoustic stimulation, the individual nanofibers, with minimized stacking and constraints, are freely vibrating in a collective manner. The nanofiber mesh, made of poly(vinylidene fluoride-*co*-trifluoroethylene) (P(VDF-TrFE)) with an average fiber diameter of ≈307 nm, is sensitive to acoustic waves from 200 to 5000 Hz, covering most of the common sound frequencies encountered in our daily life. Combining the physical merits of free-standing nanofibers in sound detection and the convenient electrical transduction mechanism of a piezoelectric polymer, this suspended P(VDF-TrFE) nanofiber mesh could enable novel applications and breakthroughs in the next-generation acoustic sensor.

The dNFES is a technique that derives from the established near-field electrospinning (NFES) process.[28,29] In dNFES, the distribution of the static field is constantly changing during the spinning process due to the presence of the electrode-pair and the air gap, inducing a dynamic switching between linear jetting and controlled whipping behaviors (as shown in **Figure 1**). The dNFES process enables to produce a suspended piezoelectric nanofiber mesh structure with in situ poling. In addition, it offers an efficient one-step fabrication, since it also provides robust in situ mechanical and electrical bonding of the fibers to the electrodes. In the dNFES process, as shown in Figure 1a–c, a pair of elevated electrodes with a 3 mm gap in between is placed on top of a translation stage. P(VDF-TrFE) solution is constantly delivered through a metallic needle located at 2 mm above the surface of the electrodes. A voltage of ≈2.5 kV is applied at the metallic needle, and the surface

of the two electrodes is grounded. The fiber spinning process starts when the needle is above the left electrode (Figure 1a). A fiber jet is produced and tethered onto the surface of the electrode due to the strong static field. When the translation stage continues to move, the static field concentrates at the edge of the electrode and the tip of the needle, as shown in the simulation depicted in Figure 1a$_1$. As a result, the fiber jet is being further stretched and thinned. When the needle is in the middle of the gap (Figure 1b), the static field distributes evenly between the two electrodes (Figure 1b$_1$); thus, the fiber jet would split and whip. The jet splitting–whipping phenomenon only happens when the static electrical forces on both sides of the electrodes acts equally to attract the fiber jet. Since the translation stage is constantly moving, this jet splitting–whipping is a transient status that lasts for less than 10 ms (as observed by high-speed imaging in Video S1 in the Supporting Information). With optimized combinations of applied static fields and electrode spacing (see further analysis below), the fiber jet whips in mid-air rather than being drawn toward the substrate of the translation stage in between the pair of electrodes. Once the needle moves closer to the other side of the electrode, the fiber jet steps and bonds, completing one cycle of the fiber spinning. The fiber bonds (≈60 µm width), serving as mechanical and electrical connections, are produced when the fiber jet writes in the "line" form on the copper electrodes. The fiber bonds are in a parallel pattern, as evidenced by scanning electron microscopy (SEM) images in Figure S1 in the Supporting Information. Repetition of the whole process leads to multiple fiber steppings on the surface of the electrodes (Figure 1c). This suspended nanofiber mesh is composed of low packing density and directional P(VDF-TrFE) nanofibers (Figure 1c$_1$,c$_2$; Figure S2, Supporting Information). The average diameter of the nanofiber is around 300 nm (307 ± 61 nm). Although the nanofiber mesh is directed to align globally, there are some interconnections among individual fibers caused by the jet splitting–whipping (Figure S2, Supporting Information). As a result, the fiber length is usually ≈10% longer than the gap distance between the pair electrodes. Beneficially, these junctions could provide structural support to enhance the stability of the suspended nanofiber network. Both ends of the nanofiber mesh are strongly attached to the electrodes without further processing, and the mesh structure spans across a gap of 3 mm.

A detailed look at the dNFES fiber spinning process, including fiber stretching, jet splitting–whipping, and fiber stepping, is captured by a high-speed camera, as shown in Figure 1d. The zoomed-in images on the right side show the jet-splitting phenomenon. The fiber jet, initially being linear and thicker when just ejected from the nozzle, starts to split into several thinner jets when reaching the height similar to the surface of the electrodes. Experimentally, we found that the static electric field, the distance between the copper electrodes, and the stage temperature are the most important parameters to obtain the desired low-stacking fiber mesh patterns with high piezoelectricity. Sufficiently high static field (>≈1 kV mm^{-1}) is necessary to initiate fiber spinning and to obtain measurable piezoelectricity (as an indication of the threshold for in situ poling) of the material. The nanofiber mesh becomes denser with increasing static field (Figure S3, Supporting Information). Particularly, when the static field is larger than 1.5 kV mm^{-1}, jet splitting and multiple jets are evidently observed (Figure S4, Supporting Information), resulting in highly entangled and dense nanofiber mesh (Figure S3c, Supporting Information). However, a field strength over 2 kV mm^{-1} would cause electrical sparks and fiber breakage, so that only very few fibers could remain suspended (Figure S5, Supporting Information). We find that a static field of ≈1.25 kV mm^{-1} could enable stable printing of suspended and piezoelectric active nanofiber mesh with satisfactory packing density (≈18%), estimated by SEM. The distance between the electrodes also affects the density of the nanofiber mesh. More fibers tend to fall in the gap with increasing distance; thus, the nanofiber mesh becomes sparse (Figure S6, Supporting Information). Usually, due to the close distance between the needle and the electrodes, it is not straightforward to obtain instant fiber solidification, and this could result in beaded fibers when fabricated at room temperature (Figure S7a,b, Supporting Information). Therefore, the translation stage is equipped with a heater to facilitate fast solvent evaporation to acquire straight fibers (Figure S7c,d, Supporting Information). We found that 60 °C is sufficient to dry the as-spun fibers after spinning, without compromising the measured piezoelectricity of the sensors.

Fourier-transform infrared spectroscopy spectrum (FTIR) in **Figure 2**a shows that the P(VDF-TrFE) nanofiber mesh contains characteristic piezoelectric β phase peaks at 1284 and 845 cm^{-1}

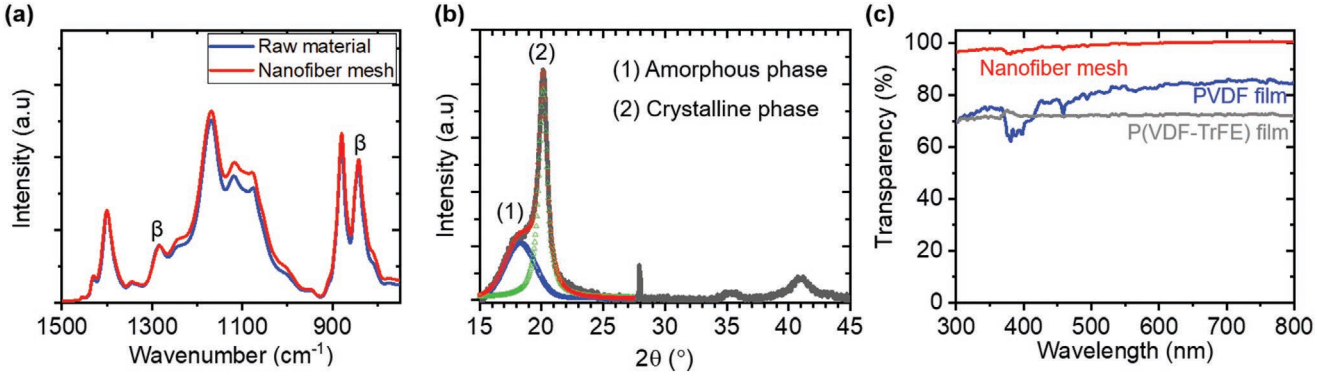

Figure 2. Compositional and physical characteristics of the P(VDF-TrFE) nanofiber mesh. a) FTIR spectroscopy of the nanofiber mesh and raw P(VDF-TrFE) powder. b) XRD spectroscopy of the nanofiber mesh. c) UV–vis spectroscopy comparing the transparency of the suspended nanofiber mesh with a commercial PVDF film (10 µm thick) and a casted P(VDF-TrFE) film (≈15 µm thick).

comparable to the raw material.[30] From X-ray powder diffraction spectrum (XRD) in Figure 2b, we have determined that the crystallinity of the nanofiber mesh is ≈66% w/w. The rich β phase and high crystallinity of the P(VDF-TrFE) nanofiber mesh make it a good candidate to achieve effective energy conversion. Compared with a commercial, semitransparent PVDF film (10 µm thickness, uniaxially oriented, GoodFellow Ltd.) and a casted P(VDF-TrFE) film (≈15 µm thickness), the suspended nanofiber mesh demonstrates superior transparency from the UV to visible light region (Figure 2c) (>97% from 380 to 700 nm region). The calculated absorption coefficients are also shown in Figure S8 in the Supporting Information for standardized transparency comparison, confirming that the dNFES nanomesh is indeed more permissive to light compared to the continuous film structures. The low packing density enables the air permissiveness and transparency of the nanofiber mesh in this work. The combination of piezoelectricity and high transparency could potentially inspire the next-generation of integrated smart home and personal devices, such as intelligent windows, wearable sensors, and breathable sensors.[31,32] Particularly, high transparency could allow convenient integration of such nanofiber mesh with optoelectronic devices, such as optical and gas sensors, potentially enabling a highly integrated sensing platform that could both "hear" and "see." Because the nanofiber mesh exhibits a permissive structure, in which the discrete, solid materials of the nanofibers only cover a small fraction of the total mesh planar area, while the remaining planar area is occupied by air, an "equivalent film thickness" is introduced to describe the mesh thickness. In a hypothetical scenario, by assuming that the discrete nanofibers are converted into a homogenous film, which covers 100% of the planar area, the thickness of this hypothetically rearranged film is defined to have an "equivalent film thickness". Based on the absorption coefficient of P(VDF-TrFE) film (estimated as ≈300 cm^{-1} at 600 nm wavelength), our P(VDF-TrFE) nanofiber mesh exhibits an equivalent film thickness of ≈60 nm. Since the P(VDF-TrFE) nanofiber mesh is optically homogenous at the tens of microlevel, and the fiber diameter is ≈307 nm, the estimated "equivalent film thickness" of the mesh (≈60 nm) further suggests that the proportional space occupied by the nanofibers is around 60/307, ≈19.5% (i.e., fiber diameter over equivalent film thickness).

A nanofiber mesh with a suspended nanofiber region of around 3 mm × 6 cm (≈1.8 cm^2) and a pair of parallel copper electrodes (width ≈2 mm) on both sides (scheme shown in Figure S9 in the Supporting Information) is used in order to test the acoustic sensing performance. The nanofiber mesh is placed at around 1 cm in front of a commercial loudspeaker (Multimedia Speaker Z150, Model S-00134) as depicted in **Figure 3**a. The acoustic waves travel perpendicular towards the nanofiber mesh, stimulating a transverse displacement. When the individual nanofibers vibrate under the acoustic field in a

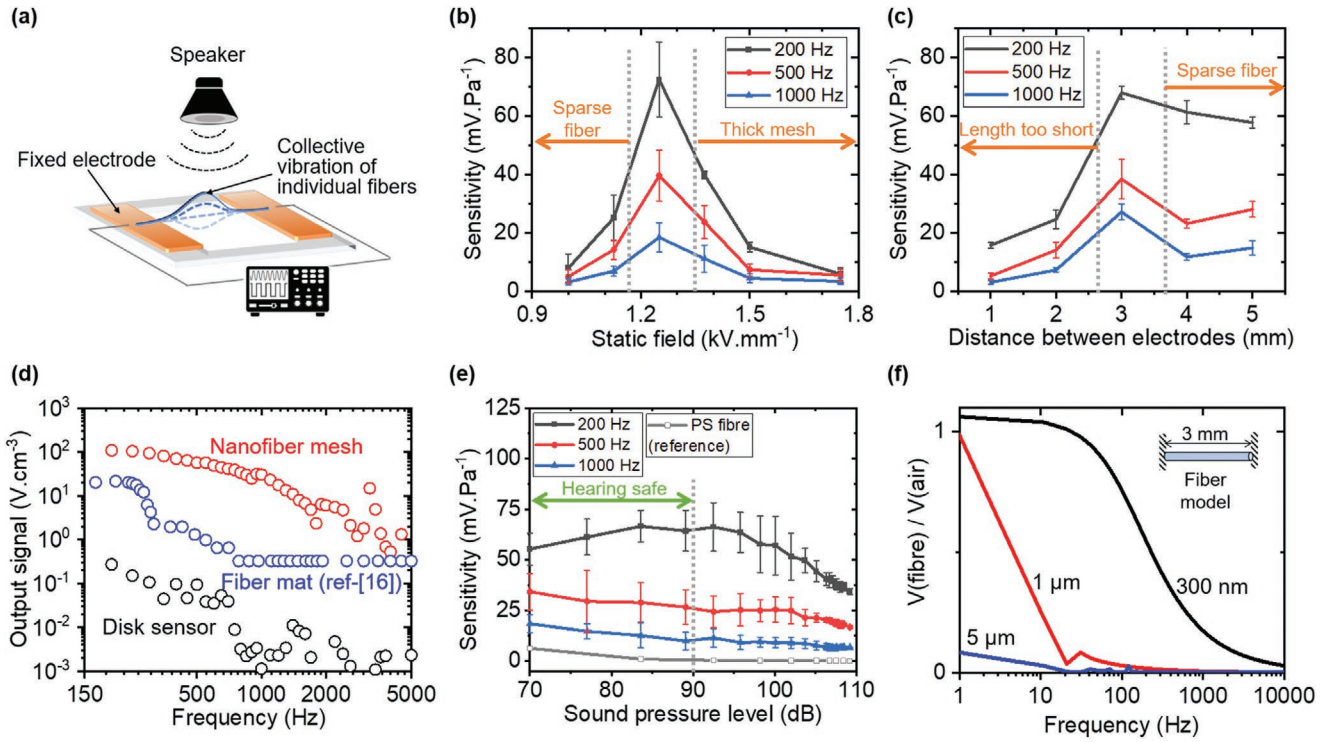

Figure 3. Acoustic sensing performance of suspended nanofiber mesh fabricated by dNFES. a) Schematic of the experimental setup. Effect of b) static field and c) distance between the electrodes on the device sensitivity at 200, 500, and 1000 Hz (tested at ≈90 dB). d) Acoustic sensing bandwidth of the nanofiber mesh ("equivalent film thickness" ≈60 nm) compared with the 40 µm thick nanofiber mat reported in literature,[16] and a commercial piezoelectric acoustic sensing dish (300 µm thick). Data is normalized in energy output density by the volume of piezoelectric materials used in the sensing device (V cm^{-3}) for cross-comparison. e) Acoustic sensitivity of the device at 200, 500, and 1000 Hz under various sound pressure levels. f) Simulation results illustrating the physical efficiency (velocity of nanofiber vs velocity of airflow) of suspended nanofiber with different diameters (in the simulation, the fiber is simplified using a fiber model of 3 mm length, and both ends are fixed).

collective manner, an output voltage is generated. The voltage signal is collected from the two copper electrodes by an oscilloscope (Tektronix TDS 2014). Figure S10 in the Supporting Information shows the signal detected with a suspended nanofiber mesh of ≈1.8 cm^2 area under a 250 Hz sound wave at ≈95 dB, and Video S2 in the Supporting Information captures the vibrations of the nanofiber mesh during the sound stimulation. The peak-to-valley value of the output voltage is ≈200 mV, of which performance compares favorably to some existing acoustic sensors based on piezoelectric polymer films and micrometer-thick fiber mats.[7,17]

We further evaluate whether the different dNFES fabrication conditions can influence the device performance, correlating to the associated nanofiber mesh morphology. Static field intensity, the distance between the electrodes, and the fabrication temperature in dNFES process are found to play essential roles in the sensitivity of the nanofiber mesh. The device sensitivity is given by Equation (1)[16]

$$S = \frac{V}{P} = \frac{V}{P_0 \times 10^{L_p/20}} \quad (1)$$

where P is the sound pressure (unit: Pa), V is the voltage output of the nanofiber mesh, P_0 is the reference sound pressure of 2×10^{-5} Pa, and L_p is the sound pressure level (SPL) in decibel (dB). As shown in Figure 3b, the best device sensitivity is found when the static field is ≈1.25 kV mm^{-1}, because a lower static field could fail to fully initiate the fiber jet, while a higher static field could result in disorientated dense fiber mat (Figure S3, Supporting Information). Theoretically, longer suspended nanofibers would have better acoustic sensing performance,[21] because they could vibrate easily without being constrained by the fixed ends. However, fibers tend to fall and become sparse when increasing the distance between the electrodes (Figure S4, Supporting Information), and experimentally, the highest sensitivity is observed when the distance between the electrodes is around 3 mm (Figure 3c). When the distance between the electrodes is smaller than 3 mm, the suspended nanofiber becomes a resonant system due to the mechanical rigidity induced by the constraints at the electrodes. Simulation results in Figure S11 in the Supporting Information, based on the physical model proposed by Zhou and Miles,[21] show that suspended nanofibers shorter than ≈1 mm become resonating systems. When the distance between the electrodes is in the range of dozens of micrometers, which is the case of the suspended nanofibers fabricated by conventional electrospinning methods,[28,29] the performance of the sensor could only be desirable at narrow frequency ranges near its resonating frequency. The effect of fabrication temperature on the device sensitivity is shown in Figure S12 in the Supporting Information. The best device sensitivity is observed when fabricated at 60 °C.

In order to assess the frequency bandwidth of the suspended P(VDF-TrFE) nanofiber mesh, a frequency sweep experiment was performed from 200 to 5000 Hz, with the speaker loudness maintained at 90 dB. A commercially available piezoelectric disk resonant acoustic sensor (300 µm thick, Piezo Discs Microphone, Sourcing Map Ltd.) is used as a comparison under the same settings. As shown in Figure 3d, the normalized output voltage (the output signal is normalized by the volume of piezoelectric materials used in the sensing device: volts per volume of the materials) of suspended nanofiber mesh maintains at a similar level from 200 to 500 Hz. Beyond 500 Hz, the output voltage starts to decrease but remains at a detectable level until 5000 Hz. This frequency bandwidth covers the most common audible sound frequency spectrum in daily life. In comparison, the output voltages of the PVDF fiber mat (40 µm thick)[16] and commercial piezoelectric disk sound sensor decreases drastically after 500 Hz. For the commercial piezoelectric disk, the normalized voltage output approaches zero beyond ≈800 Hz. Thus, the mechanical rigidity and bulky morphology of the PVDF film result in a strong resonant phenomenon, which inevitably restricts the sensitive frequency bandwidth. Overall, the nanofiber mesh acoustic sensor clearly outperforms existing film-like structures in widening the frequency bandwidth, which can also be described by the quality factor (Q factor). Q factor is defined as $f_0/\Delta f$ (resonant or maxima frequency over full width at half maxima). Lower values of Q factor indicate broader frequency coverage. The Q factor of P(VDF-TrFE) nanofiber mesh is 0.49, while the Q factor of the commercial piezoelectric disk sound sensor is 3.01 (thus, the nanofiber mesh is around five times better). The fact that the nanofiber mesh provides broadband sensing beyond 1000 Hz could enable practical sound sensing applications. For example, in the recording fidelity of nontonal languages (such as English), the consonants are important. The consonants are predominantly found in the frequency range above 500 Hz, and more specifically, in the 2–4 kHz frequency range,[33] which is out of the sensitivity range of the fiber mat and the commercial sensor. The effect of the SPL on the sensitivity of the P(VDF-TrFE) nanofiber mesh at 200, 500, and 1000 Hz is shown in Figure 3e. As a reference, nonpiezoelectric fibers (polystyrene (PS)) fabricated by dNFES as a negative control has been added to reflect the noise level. The voltage output is shown in Figure S13 in the Supporting Information. The optimal acoustic sensitivity of the nanofiber mash is found in the 60–90 dB hearing-safe SPL level, which makes it suitable for sensing applications in daily life and field applications. The noise level collected by the nonpiezoelectric PS fibers is less than 1.5 mV from 60 to 110 dB, and the signal to noise ratio is ≈6 at 60 dB and ≈133 at 110 dB (200 Hz). Additionally, the human voice is used as the sound source to test the response of the device (Figure S14, Supporting Information), showing that the device was responsive at normal human voice levels in the ambient environment. This further proves that the signals detected are not due to electromagnetic interferences of the speaker.

Since the vibration of the nanofiber mesh is driven by the fluidic forces of low-viscosity and low-density air, the fiber diameter is expected to play a key role in the acoustic bandwidth sensitivity of the fiber device. In order to evaluate such effect, simulation based on the physical models proposed by Miles and Zhou is used to exam the physical efficiency (the ratio between the velocity of the fiber over the velocity of the airflow: V_{fiber}/V_{air}) of individual nanofibers of different diameters in response to the air fluctuation induced by acoustic waves.[22] The fiber is modeled as a 3 mm long structure with both ends fixed. As shown in Figure 3f, a microfiber (5 µm diameter) fails to move with air fluctuation because the fluidic force in the acoustic field is too weak to drive their motion. A fiber of 1 µm

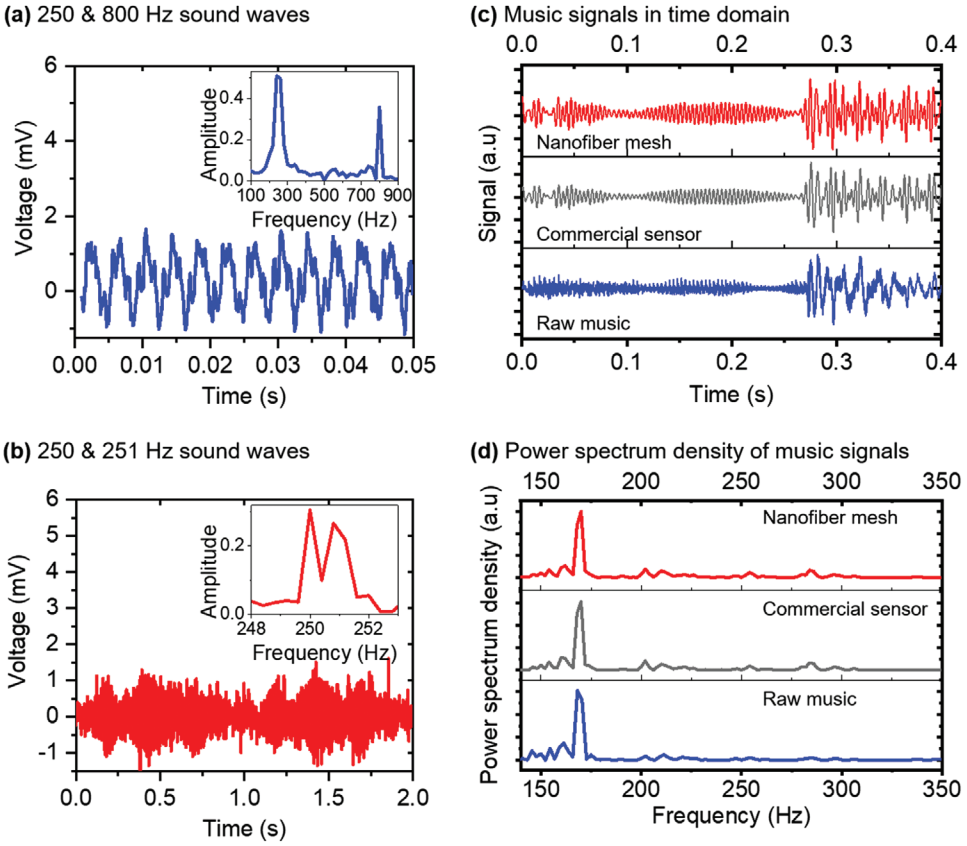

Figure 4. Acoustic sensing fidelity. a,b) Signal output of nanofiber mesh at two interfering frequencies at 70 dB, and the FFT processed spectrum. c) Signal output in time domain and d) the corresponding power spectrum density data of the nanofiber mesh and the commercial sensor in recording a piece of music.

diameter possesses high physical efficiency ($V_{fiber}/V_{air} \approx 1$) in the low frequency range (<20 Hz), while the efficiency is almost lost in the sound voice region (frequency higher than 300 Hz). A fiber of 300 nm maintains reasonably high physical efficiency across the major region of the audible sound frequency spectrum. Typical reported MEMS microhair and microarray-based acoustic sensors usually have free-standing dimensions in the range of several micrometers; thus they are not able to work as efficiently as suspended nanofiber mesh, especially for wide frequency bandwidth detection.

The ability to distinguish different frequencies in sound is another important characteristic of the acoustic sensor. Under two frequencies input of 250 and 800 Hz (**Figure 4**a), the nanofiber mesh could differentiate them, as shown in the insert showing its associated fast Fourier transform (FFT) processing. Even under two similar input sound frequencies (250 and 251 Hz), the nanofiber mesh could still be able to differentiate them, as shown in Figure 4b. In the case of mixed-frequency detection, the FFT treatment shows that the nanofiber mesh could clearly detect different frequencies (Figure S15, Supporting Information).

Finally, we demonstrate that the dNFES suspended nanofiber mesh has high fidelity in reproducing the acoustic signals detected. A piece of music is used to test if the nanofiber mesh could reproduce the signals. As shown in Figure 4c comparing the raw music signal with the signals detected by the fiber mesh and the commercial piezoelectric sensor, the signals detected by the fiber mesh clearly resemble the key features and details in the raw music files. The power spectrum density showing the signal comparison in the frequency domain is shown in Figure 4d and Figure S16 in the Supporting Information (in log–log scale). An entire music piece of 4 minutes can be recorded continuously (Video S3, Supporting Information).

In summary, we demonstrate the first suspended low packing density piezoelectric nanofiber mesh acoustic sensor fabricated by an original dNFES technique. Thanks to the unique electrode and spinning configuration that lead to controlled jet whipping, dNFES achieves efficient fabrication of suspending and directional P(VDF-TrFE) nanofiber mesh along with in situ poling. Compared with conventional resonant acoustic sensors, this nanofiber mesh recapitulates the high aspect ratio, ultrathin, and free-standing morphology of nonresonating acoustic sensing structure, leading to a self-powered, broad bandwidth sensing system. The nanoscale dimension (≈307 nm fiber diameter) and freely suspended nature of the sensing platform enable the collective vibration of the nanofiber mesh to be efficiently driven by air fluctuations under acoustic waves at a broad frequency bandwidth. Practical performances, including device sensitivity at hearing-safe SPL and high fidelity in signal recording, have been demonstrated especially in the low and middle-frequency ranges that are widely present in our daily life. In the future, such a broadband piezoelectric

nanomesh sound sensor, with its unique transparency and permissiveness, may be combined with gas and optical sensors for multidimensional information collection within the same smart device platform.

Experimental Section

Solution Preparation and dNFES Setup: The solution for fiber spinning was prepared by dissolving 0.46 g P(VDF-TrFE) powders (Solvene 250/P300, Sigma-Aldrich) in a 2.5 mL solvent mixture of 1.5 mL DMF (Sigma-Aldrich) and 1 mL acetone (Sigma-Aldrich), and then the solution was stirred at room temperature for 12 h. The dNFES setup consisted of a set of X-Y linear translation stages (DDSM100/M, Thorlabs) for fiber spinning, and a vertical Z stage to adjust the distance between the elevated electrodes and the needle (L490MZ/M, Thorlabs). The solution was delivered through a 30-gauge blunt end stainless steel needle at a flow rate of 100 µL h^{-1}. The needle was connected to a high voltage supply at 2.5 kV, and the top surfaces of the elevated electrodes were grounded. During fiber spinning, the translation stage was constantly heated at 60 °C, and the translation speed of the X-Y stage was at 70 mm s^{-1}. The high-speed images of the fiber spinning process were taken by a PHANTOM VEO-E 310L high-speed camera.

Electrical Field Simulation in dNFES: The finite element analysis of the static field in Figure 1 was simulated with Ansys 19.1 Workbench Steady-State Electric Conduction mode. Multiple models with the needle being at different positions relative to the electrodes were created and analyzed individually. The size of the needle (30-gauge), the distance between the electrodes (3 mm), and the distance between the needle and the electrodes (2 mm) were set as actual values. The surface of the needle was set as 2.5 kV, and the surfaces of the electrodes were set as 0 V. The ambient material was air, with a density of 1.225 kg m^3, resistivity of 2×10^{16} Ω m, and dielectric constant of 1.

Fiber Mesh Characterizations: The morphologies of the P(VDF-TrFE) nanofiber meshes were examined by environmental SEM (Helios FIB/SEM) at an accelerator voltage of 1 kV. The packing density was estimated from SEM images of the fiber mesh in three different regions using MATLAB image segmentation tool (Figure S17, Supporting Information). Pixels that occupied by the nanofibers were identified and then divided by the overall pixels of the image. The actual length of the fiber was estimated from the combination of SEM and optical images. Suspended fiber meshes were collected and squeezed into small flasks in order to acquire FTIR (Frontier, PerkinElmer) and XRD (Bruker D8 Advance powder X-ray diffractometer) spectroscopies. The degree of crystallinity (DOC %) was estimated by $DOC = A_c/(A_c + A_a)$, where A_c represents the crystalline areas and A_a the amorphous area.[34] In the UV–vis spectroscopy, suspended fiber mesh was directly used in JENWAY 7205 Spectrometer. By assuming that the nanofiber mesh and the P(VDF-TrFE) film have the same absorption coefficient α at 600 nm wavelength ($\alpha = 2.303 \times A_{film}/t_{film}$, where A_{film} and t_{film} are the absorbance and thickness of the P(VDF-TrFE) film), the "equivalent film thickness" of nanofiber mesh was estimated by $t_{fiber} = 2.303 \times A_{fiber}/\alpha$.

Acoustic Sensing Performance Characterization: A commercial loudspeaker was used as the sound source, and the acoustic signals were generated through a sinusoidal signal generator with MATLAB. The setup is depicted in Figure S18a in the Supporting Information. The suspended nanofiber mesh was placed at around 10 mm in front of the speaker diaphragm. An oscilloscope was used to collect the piezoelectric signals. In order to eliminate the noise signals from the environment and other instruments, the nanofiber mesh was shielded inside a Faraday Cage made of copper mesh. The frequency was tuned from 200 to 5000 Hz to assess the detectable frequency bandwidth of suspended P(VDF-TrFE) nanofiber mesh sensing devices. The sound loudness in the place where fiber mesh was placed was measured with a decibel sound meter (Sauter SU 130 Sound Level Meter). In order to assess the sensing resolution of the nanofiber mesh in distinguishing two different acoustic signals, two separate identical speakers were used to play sounds of specific frequencies (Figure S18b, Supporting Information). In Figure 3d, the output signal per unit volume was normalized by the volume of piezoelectric materials used in the sensing device. The nanofiber mat had an area of 12 cm^2 and thickness of 40 µm; thus, the material volume was 4.8×10^{-3} cm^3, and the commercial sensor had an area of 9.6 cm^2 and thickness of 300 µm; thus, the material volume was 28.8×10^{-3} cm^3. The nanofiber mesh had an area of 1.8 cm^2, and the thickness was 307 nm, considering the packing density of 18%. Thus, the resulted material volume was 9.2×10^{-7} cm^3.

Supporting Information

Supporting Information is available from the Wiley Online Library or from the author.

Acknowledgements

This work was supported by the European Research Council (ERC-StG, 758865). W.W. is grateful for the support from the Chinese Scholarship Council. P.N.S. thanks Prof. Bradley Nelson and his group in the Institute of Robotics and Intelligent Systems in ETH for support and guidance.

Conflict of Interest

The authors declare no conflict of interest.

Keywords

bioinspired acoustics, energy harvesting, nanogenerators, nanosensors, P(VDF-TrFE)

Received: January 29, 2020
Revised: April 18, 2020
Published online: June 8, 2020

[1] J. Yang, J. Chen, Y. Liu, W. Yang, Y. Su, Z. L. Wang, *ACS Nano* **2014**, *8*, 2649.
[2] X. Fan, J. Chen, J. Yang, P. Bai, Z. Li, Z. L. Wang, *ACS Nano* **2015**, *9*, 4236.
[3] Y. Hu, E. G. Kim, G. Cao, S. Liu, Y. Xu, *Ann. Biomed. Eng.* **2014**, *42*, 2264.
[4] Y. H. Jung, S. K. Hong, H. S. Wang, J. H. Han, T. X. Pham, H. Park, J. Kim, S. Kang, C. D. Yoo, K. J. Lee, *Adv. Mater.* **2019**, https://doi.org/10.1002/adma.201904020.
[5] J. H. Han, K. M. Bae, S. K. Hong, H. Park, J. H. Kwak, H. S. Wang, D. J. Joe, J. H. Park, Y. H. Jung, S. Hur, C. D. Yoo, K. J. Lee, *Nano Energy* **2018**, *53*, 658.
[6] M. Liu, X. Pu, C. Jiang, T. Liu, X. Huang, L. Chen, C. Du, J. Sun, W. Hu, Z. L. Wang, *Adv. Mater.* **2017**, *29*, 1703700.
[7] J. Park, M. Kim, Y. Lee, H. S. Lee, H. Ko, *Sci. Adv.* **2015**, *1*, e1500661.
[8] L. Q. Tao, H. Tian, Y. Liu, Z. Y. Ju, Y. Pang, Y. Q. Chen, D. Y. Wang, X. G. Tian, J. C. Yan, N. Q. Deng, Y. Yang, T. L. Ren, *Nat. Commun.* **2017**, *8*, 14579.
[9] D. Floreano, R. J. Wood, *Nature* **2015**, *521*, 460.
[10] J. Jang, J. H. Jang, H. Choi, *Adv. Healthcare Mater.* **2017**, *6*, 1700674.
[11] S. Roundy, P. K. Wright, J. Rabaey, *Comput. Commun.* **2003**, *26*, 1131.
[12] H. S. Lee, J. Chung, G. T. Hwang, C. K. Jeong, Y. Jung, J. H. Kwak, H. Kang, M. Byun, W. D. Kim, S. Hur, S. H. Oh, K. J. Lee, *Adv. Funct. Mater.* **2014**, *24*, 6914.

[13] H. Droogendijk, J. Casas, T. Steinmann, G. J. M. Krijnen, *Bioinspiration Biomimetics* **2015**, *10*, 016001.
[14] B. Stadlober, M. Zirkl, M. Irimia-Vladu, *Chem. Soc. Rev.* **2019**, *48*, 1787.
[15] T. H. Lee, C. Y. Chen, C. Y. Tsai, Y. K. Fuh, *Polymers* **2018**, *10*, 692.
[16] C. Lang, J. Fang, H. Shao, X. Ding, T. Lin, *Nat. Commun.* **2016**, *7*, 11108.
[17] J. H. Han, J. H. Kwak, D. J. Joe, S. K. Hong, H. S. Wang, J. H. Park, S. Hur, K. J. Lee, *Nano Energy* **2018**, *53*, 198.
[18] N. Chocat, G. Lestoquoy, Z. Wang, D. M. Rodgers, J. D. Joannopoulos, Y. Fink, *Adv. Mater.* **2012**, *24*, 5327.
[19] S. N. Cha, J. S. Seo, S. M. Kim, H. J. Kim, Y. J. Park, S. W. Kim, J. M. Kim, *Adv. Mater.* **2010**, *22*, 4726.
[20] R. Que, Q. Shao, Q. Li, M. Shao, S. Cai, S. Wang, S. T. Lee, *Angew. Chem., Int. Ed.* **2012**, *51*, 5418.
[21] J. Zhou, R. N. Miles, *Proc. Natl. Acad. Sci. USA* **2017**, *114*, 12120.
[22] R. N. Miles, J. Zhou, *J. Vib. Acoust.* **2018**, *140*, 011009.
[23] J. Zhou, B. Li, J. Liu, W. E. Jones, R. N. Miles, *J. Micromech. Microeng.* **2018**, *28*, 095003.
[24] J. Xu, M. J. Dapino, D. Gallego-Perez, D. Hansford, *Sens. Actuators, A* **2009**, *153*, 24.
[25] K. Maity, B. Mahanty, T. K. Sinha, S. Garain, A. Biswas, S. K. Ghosh, S. Manna, S. K. Ray, D. Mandal, *Energy Technol.* **2017**, *5*, 234.
[26] Y. Jiang, L. Gong, X. Hu, Y. Zhao, H. Chen, L. Feng, D. Zhang, *Polymers* **2018**, *10*, 364.
[27] S. H. Park, H. B. Lee, S. M. Yeon, J. Park, N. K. Lee, *ACS Appl. Mater. Interfaces* **2016**, *8*, 24773.
[28] C. Chang, V. H. Tran, J. Wang, Y. K. Fuh, L. Lin, *Nano Lett.* **2010**, *10*, 726.
[29] X. Wang, G. Zheng, G. He, J. Wei, H. Liu, Y. Lin, J. Zheng, D. Sun, *Mater. Lett.* **2013**, *109*, 58.
[30] D. Mandal, S. Yoon, K. J. Kim, *Macromol. Rapid Commun.* **2011**, *32*, 831.
[31] A. Miyamoto, S. Lee, N. F. Cooray, S. Lee, M. Mori, N. Matsuhisa, H. Jin, L. Yoda, T. Yokota, A. Itoh, M. Sekino, H. Kawasaki, T. Ebihara, M. Amagai, T. Someya, *Nat. Nanotechnol.* **2017**, *12*, 907.
[32] X. Yu, R. Rajamani, K. A. Stelson, T. Cui, *Sens. Actuators, A* **2006**, *132*, 626.
[33] B. C. J. Moore, M. A. Stone, C. Füllgrabe, B. R. Glasberg, S. Puria, *Ear Hear.* **2008**, *29*, 907.
[34] J. H. Bae, S. H. Chang, *Compos. Struct.* **2015**, *131*, 1090.